Optical and Quantum Electronics (2020) 52:95
https://doi.org/10.1007/s11082-019-2173-5

Multifractal and optical bandgap characterization of Ta_2O_5 thin films deposited by electron gun method

Reza Shakoury[1] · Sahar Rezaee[2] · Fredrick Mwema[3,4] · Carlos Luna[5] · Koushik Ghosh[6] · Stanislav Jurečka[7] · Ştefan Ţălu[8] · Ali Arman[9] · Alireza Grayeli Korpi[10]

Received: 12 September 2019 / Accepted: 21 December 2019
© Springer Science+Business Media, LLC, part of Springer Nature 2020

Abstract
The micromorphology of tantalum pentoxide (Ta_2O_5) thin films, deposited on glass substrates by electron gun method, has been analyzed using atomic force microscopy (AFM), UV–Vis–NIR spectrophotometry and multifractal analyses. Two samples were grown at basic pressure of 7×10^{-6} mbar, work pressures of 1.3×10^{-4} and 2.0×10^{-4} mbar, and thicknesses of 0.38 µm and 0.39 µm, respectively. Subsequently, these samples were annealed at 300 °C for 2 h. The physical, structural and optical analyses were investigated by spectroscopic ellipsometry, spectrophotometry and AFM. The measured transmittance spectra were studied based on the Swanepoel method, whose results also yielded to the estimation of the film thickness and the refractive index. Finally, Ta_2O_5 thin films were characterized by AFM measurements and multifractal analyses for an accurate description of the 3-D surface microtexture features. The fractal examinations of the samples revealed that these microstructures exhibit multifractal characteristics. Essential parameters that characterized the thin films were compared and discussed thoroughly.

Keywords Atomic force microscopy · Electron gun method · Multifractal analysis · Optical properties · Ta_2O_5 thin films

1 Introduction

Tantalum pentoxide (Ta_2O_5) thin films have wide applications in the semiconductor industry, and as such, it has been extensively studied throughout decades (Chaneliere et al. 1998). They have excellent antireflective properties, which make them suitable for optical and photovoltaic applications. On the other hand, Ta_2O_5 has a high dielectric constant and it is highly compatible with microelectronic materials, finding a variety of uses such as gate dielectrics in capacitors for new generation memory components (Prasanna et al. 2014; Lin et al. 2003).

✉ Sahar Rezaee
Saharrezaee593@iauksh.ac.ir

Extended author information available on the last page of the article

Published online: 29 January 2020

These films also have high UV transparency, high transmittance, high ionic conductivity and high thermal and chemical stability; consequently, they are broadly used as solid electrolytes in five-layer electrochromic cells (Wang et al. 2011). The electrochromic devices are extensively used in smart windows, smart energy buildings, reflectance and switchable mirrors, and smart displays (Chen et al. 2018). Due to these novel applications, a lot of research has been conducted on the deposition and characterization of Ta_2O_5 thin films.

Several methods have so far been used to prepare these films for various applications, including chemical vapor deposition (Lin et al. 2003; Siodmiak et al. 2000; Lee et al. 2003; Kaliwoh et al. 2002; Porporati et al. 2003), sputtering (Prasanna et al. 2014; Wang et al. 2011; Shibata 1996), electron beam vaporization (Porqueras et al. 1999; Prachachet et al. 2017; Tian et al. 2019; Yoon et al. 2005, 2008) and pulsed laser deposition (Han et al. 2015), among others.

The sputtering technique has been used considerably (Wang et al. 2011). Ion-beam deposition is another attractive method for preparing Ta_2O_5 films since it has been proved to make low scattering films, and the process can be tuned because the process involves the atom-by-atom transport in low pressure conditions (Mikhelashvili and Eisenstein 1999). The process has been shown to form thin films with a higher packing density closer to the bulk materials. It enhances the adhesion of the films onto the substrate (Yoon et al. 2005).

Surface topography of thin films plays a critical role in their performance and functionality (Mwema et al. 2019). It influences their electrical, corrosion, wear and optical properties (Stach et al. 2017; Kaspar et al. 2019).

Surface topography is directly related to the growth mechanism of thin films. Therefore, acquiring topographic information of thin films is of crucial importance to understand the growth principles of the deposition method, as well as the functionality of the films (Shikhgasan et al. 2015; Naseri et al. 2017; Dallaeva et al. 2014; Dastan et al. 2016).

Topography information is generally obtained through scanning tunneling techniques, with atomic force microscopy (AFM) being the most preferred over the other methods due to its versatility and flexibility (Sobola et al. 2017; Konsek et al. 2018; Shakoury et al. 2019). Also, the information obtained from AFM images has been used to determine the statistical and lateral roughness of the films using the power spectrum density functions (Stach et al. 2015; Ţălu 2015).

Surface analyses of the three-dimensional (3-D) surface morphology at nanoscale have been introduced, such as stereometric (Stach et al. 2017; Mwema et al. 2018), Minkowski functionals (Korpi et al. 2019), fractal (Zavarian et al. 2017; Arman et al. 2015; Ţălu et al. 2014), and multifractal (Ţălu et al. 2014, 2019; Yadav et al. 2015) methods. Despite a lot of published reports on the deposition and characterization of Ta_2O_5 thin films, there are very few studies about the multifractal characteristics of such thin films.

In this article, we present a detailed analysis of the 3-D micromorphology of electron beam evaporation Ta_2O_5 thin films based on AFM, UV–Vis-NIR spectrophotometry and multifractal analyses.

2 Experimental section

Ta_2O_5 thin films were deposited on glass substrates through the electron gun method. The deposition facility is equipped with two oil-free rotary and diffusion vacuum pumps. A schematic illustration of the electron gun evaporator is shown in Fig. 1.

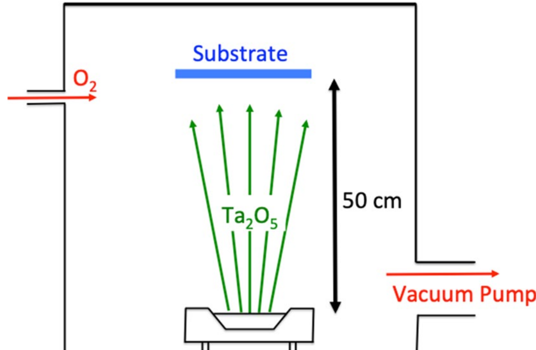

Fig. 1 Schematic diagram of electron gun deposition setup

Two samples were deposited at different deposition rates and working pressure to obtain sample #1 and #2. The details of the experimental parameters and samples are summarized in Table 1.

A quartz microbalance controlled the deposition rate and film thickness. In the used setup, argon gas acts as the working gas to maintain the vacuum pressure inside the deposition chamber, whereas oxygen gas is fed next to the glass substrate for reactive processes to occur effectively. The target consisted of pure tantalum pentoxide (99.99%) was located at 500 mm from the substrate. The deposition rate was maintained at 2 nm/s, and the deposition was undertaken at pressure of 7×10^{-6} mbar. After deposition, the films were annealed at 300 °C in a vacuum furnace for 2 h.

The samples were then sliced 10 mm by 10 mm for AFM imaging.

The UV–visible spectra were recorded using a Hitachi 3501 model UV–Visible/NIR spectrophotometer. The thickness and the refractive index of the Ta_2O_5 thin films were estimated from these data using the Swanepoel method (Swanepoel 1983; Sánchez-González et al. 2006; Korpi et al. 2017).

In this manner, the refractive index, $n=n(\lambda)$, was calculated using the following equation (Sánchez-González et al. 2006; Korpi et al. 2017):

$$n = \sqrt{N + \sqrt{N^2 - s^2}} \tag{1}$$

where $N=N(\lambda)$ is the refraction number, s is the substrate refractive index, and λ is the wavelength of the electromagnetic radiation.

The refraction number was calculated using the following equation (Korpi et al. 2017):

Table 1 Preparation details of the deposited samples

No.	Target	Thickness (nm)	Rate (nm/s)	Basic pressure (mbar)	Work pressure (mbar)	Annealing temperature (°C)	
						–	Time (h)
#1	Ta_2O_5	380	2	7×10^{-6}	1.3×10^{-4}	300 °C	2
#2	Ta_2O_5	390	2	7×10^{-6}	2×10^{-4}	300 °C	2

$$N(\lambda) = 2s\frac{T_M(\lambda) - T_m(\lambda)}{T_M(\lambda) \cdot T_m(\lambda)} + \frac{s^2 + 1}{2} \tag{2}$$

where $T_M = T_M(\lambda)$ and $T_m = T_m(\lambda)$ are the transmittance maxima and minima of the interference fringes.

The film thickness was determined from the interference fringes observer in the transmittance spectra using the following formula (Sánchez-González et al. 2006):

$$t = \frac{\lambda_1 \lambda_2}{2[\lambda_2 n(\lambda_1) - \lambda_1 n(\lambda_2)} \tag{3}$$

where λ_1 and λ_2 are the wavelengths corresponding to two adjacent maxima or minima of the transmittance, respectively.

The direct transition optical band gap energy, E_g, of the four samples was calculated from Tauc´s plot analysis using the equation (Alijani et al. 2017; Luna et al. 2016; Rezaee and Ghobadi 2018; Ghobadi and Rezaee 2016):

$$\alpha \cdot h \cdot v^2 = A(h \cdot v - E_g) \tag{4}$$

where α is the absorption coefficient, h is the Plank´s constant, υ is the frequency of the photons and A is a parameter independent of the photon energy.

The absorption coefficient exhibits a tail near the band edge describing an exponential dependence on photon energy (Ilican et al. 2008):

$$\alpha = \alpha_0 \exp\left(\frac{h \cdot v - E_0}{E_U}\right) \tag{5}$$

where α_0 and E_0 are constants, and E_U is the Urbach energy.

3 Results and discussion

The deposition of Ta_2O_5 layers and the annealing treatments modify the surface morphology of samples grown by electron beam evaporation. AFM images of formed structures prepared in this work before and after the annealing treatment are shown in Fig. 2.

We represented the surface morphology by the random height function $h(x, y)$ and studied its properties by fractal geometry methods (Ţălu 2015).

In order to avoid the influence of the $h(x, y)$ outliers on the multifractal characteristics, we selected rectangular areas of 1.66 × 2.0 μm^2 (as shown in Fig. 3) and computed the multifractal singularity spectrum, $f(\alpha)$, and the generalized fractal dimension, D_q (Chhabra et al. 1989). These functions provide sensitive information about changes in the surface morphology connected with the surface treatment.

Details of multifractal singularity spectra and Dq dimension are shown in Figs. 4 and 5.

The obtained $f(\alpha)$ and D_q functions indicate multifractal properties related to changes in the self-similarity and scaling properties of observed surface features. With increasing of the working pressure in the deposition procedure from 1.3×10^{-4} mbar (sample a) to 2×10^{-4} mbar (sample c), the $f(\alpha)$ changes very drastically and the fractal structure significantly decreases as can be seen in Figs. 4a and 3c. This trend is also illustrated by changes in the D_q values in Fig. 5a, c, where less steep decreasing trend of the D_q values show lower multifractality. The annealing at 300 °C of the Ta_2O_5 layers completely

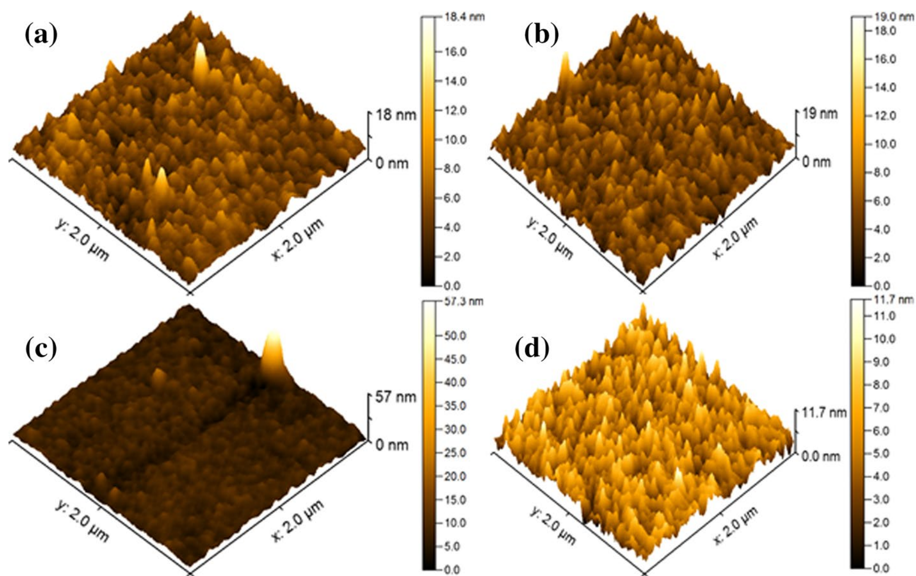

Fig. 2 3-D AFM micrographs of **a** Ta_2O_5 before annealing (1.3×10^{-4} mbar), **b** Ta_2O_5 annealed at 300 °C (1.3×10^{-4} mbar), **c** Ta_2O_5 before annealing (2×10^{-4} mbar), **d** Ta_2O_5 annealed at 300 °C (2×10^{-4} mbar)

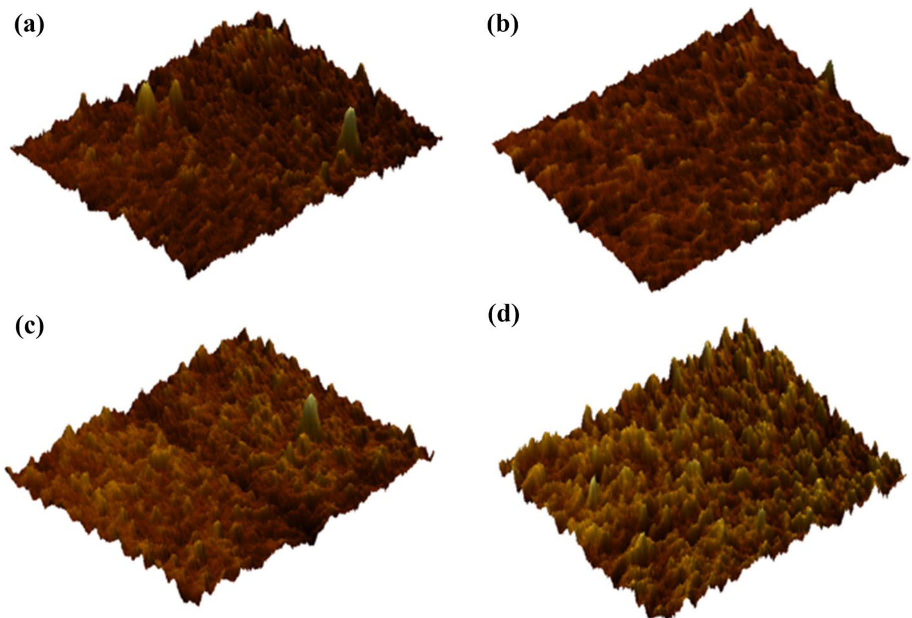

Fig. 3 AFM micrographs of selected surface area ($1.66\times2\ \mu m^2$) for the multifractal analysis: **a** Ta_2O_5 before annealing (1.3×10^{-4} mbar), **b** Ta_2O_5 annealed at 300 °C (1.3×10^{-4} mbar), **c** Ta_2O_5 before annealing (2×10^{-4} mbar), **d** Ta_2O_5 annealed at 300 °C (2×10^{-4} mbar)

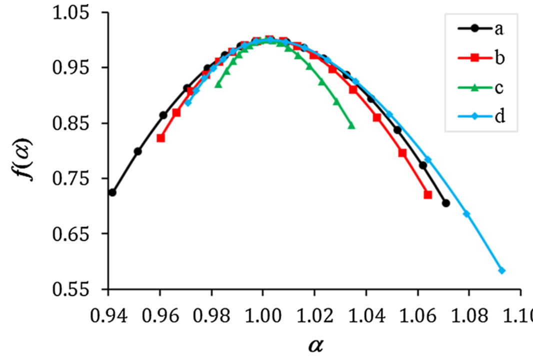

Fig. 4 Multifractal spectra graphs ($f(\alpha)$ versus α) of: (a) Ta_2O_5 before annealing (1.3×10^{-4} mbar), (b) Ta_2O_5 annealed at 300 °C (1.3×10^{-4} mbar), (c) Ta_2O_5 before annealing (2×10^{-4} mbar), (d) Ta_2O_5 annealed at 300 °C (2×10^{-4} mbar). Momentum values q are set from -8 to $+8$

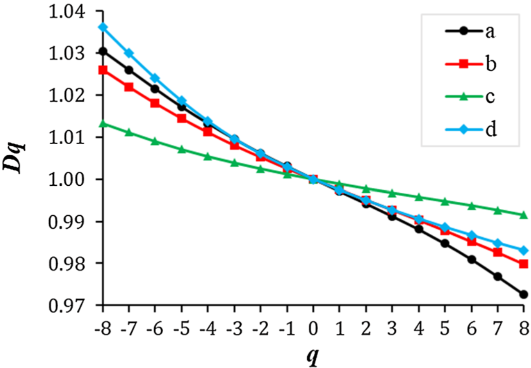

Fig. 5 Generalized fractal dimension D_q versus q of (a) Ta_2O_5 before annealing (1.3×10^{-4} mbar), (b) Ta_2O_5 annealed at 300 °C (1.3×10^{-4} mbar), (c) Ta_2O_5 before annealing (2×10^{-4} mbar), (d) Ta_2O_5 annealed at 300 °C (2×10^{-4} mbar)

Table 2 The properties of multifractal singularity spectra $f(\alpha)$ and generalized fractal dimension D_q

Sample	$\alpha_{max}-\alpha_{min}$	$f(\alpha_{min})-f(\alpha_{max})$	$D_q(-8)-D_q(8)$
(a) Ta_2O_5 before annealing (1.3×10^{-4} mbar)	0.129	0.019	0.058
(b) Ta_2O_5 annealed at 300 °C (1.3×10^{-4} mbar)	0.104	0.102	0.046
(c) Ta_2O_5 before annealing (2×10^{-4} mbar)	0.052	0.074	0.022
(d) Ta_2O_5 annealed at 300 °C (2×10^{-4} mbar)	0.122	0.303	0.053

reverses this trend. In Fig. 4b (annealed sample a) and Fig. 4d (annealed sample b), we observe increasing values of the multifractal singularity spectra, and in Fig. 5b, d pronounced fractality of annealed Ta_2O_5 structures (a) and (b). Annealing procedure produces surface features with increased self-similarity and scaling property.

The width of the $f(\alpha)$ curve, $\Delta\alpha=(\alpha_{max}-\alpha_{min})$, corresponds to the shape variability of the morphological objects. The variability of the morphological objects slightly decreases after annealing of sample a) but significantly increases after annealing of sample b).

Ta_2O_5 structures formed under higher working pressure show a substantially increased variability of morphological objects after the annealing treatment (according to the development of $f(\alpha)$ curves in Fig. 4 and $\Delta\alpha$ values in Table 2). Furthermore, the symmetry of the $f(\alpha)$ curves represented by $\Delta f=f(\alpha_{min})-f(\alpha_{max})$ values, indicate the degree of structural

non-uniformity. Δf is different for all observed structures (as it is observed in Table 2) and it increases with the sample annealing.

Generalized fractal dimension D_q curves are shown in Fig. 4. The decreasing shape of the D_q curves observed for all Ta_2O_5 structures is typical for multifractal systems and is more marked for structures formed under higher working pressure.

Figure 6 shows the transmittance and absorption spectra of the four studied samples. It is observed that the oscillations of these spectra are shifted to higher wavelengths in the annealed samples with respect to the respective untreated samples. On the other hand, the as-prepared sample obtained with a work pressure of 1.3×10^{-4} mbar presents oscillations slightly shifted to higher wavelengths in comparison with those of the spectrum of the untreated sample obtained with a work pressure of 2×10^{-4} mbar. The average transmittance of the samples at wavelengths between 400 and 1000 nm is around 80% for all samples.

The refractive index and the film thickness were calculated from the transmittance data following the method proposed by Swanepoel (Swanepoel 1983). For this, the positions of peak maxima and peak minima of transmittance were interpolated to a parabolic function to obtain the maximum $T_M(\lambda)$ and minimum $T_m(\lambda)$ transmittance envelope curves respectively (as shown in Fig. 7), as it is described in reference (Sánchez-González et al. 2006).

From these envelope curves, the refraction number is calculated using the Eq. (2), and with the obtained function $N=N(\lambda)$, the refractive index $n(\lambda)$ is determined as a function of the radiation wavelength using the expression (1). In Fig. 8 are shown the computed results.

The film thickness of the four samples was calculated from the refractive index corresponding to adjacent transmittance maxima values (or minima values) using the Eq. (3). The average of the film thickness values obtained and the corresponding standard

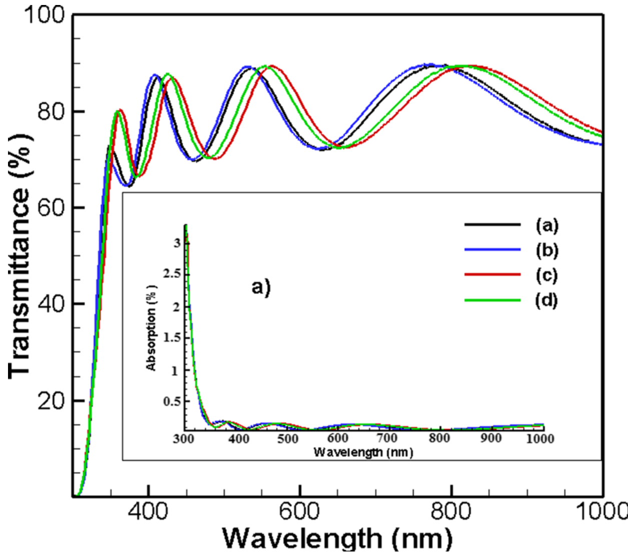

Fig. 6 Transmittance and absorbance spectra (inset a) of (a) Ta_2O_5 before annealing (1.3×10^{-4} mbar), (b) Ta_2O_5 annealed at 300 °C (1.3×10^{-4} mbar), (c) Ta_2O_5 before annealing (2×10^{-4} mbar), (d) Ta_2O_5 annealed at 300 °C (2×10^{-4} mbar)

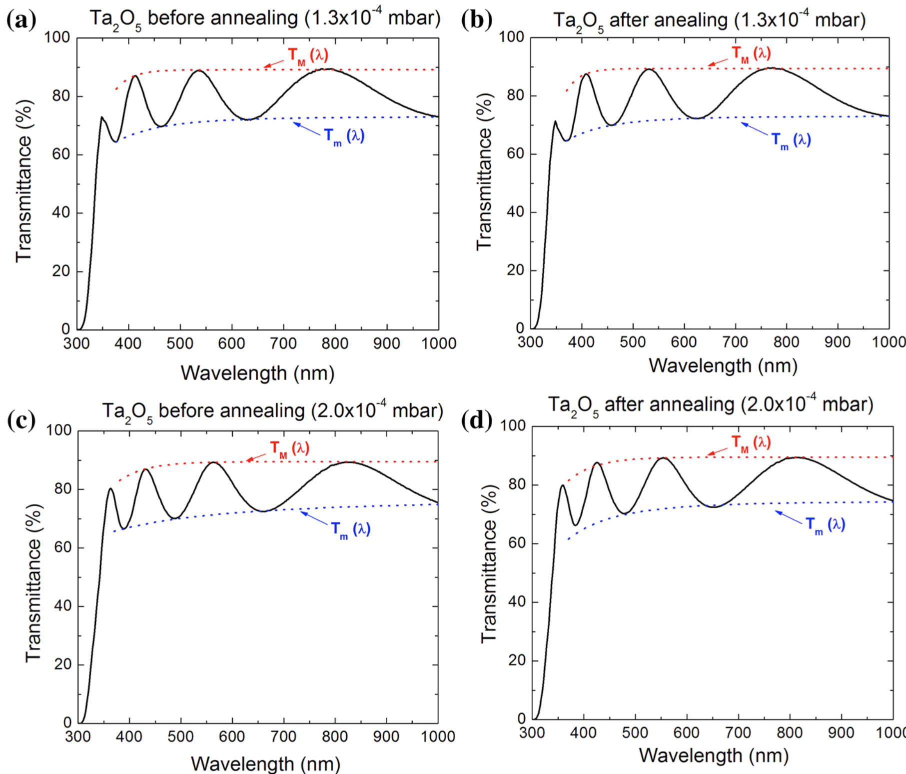

Fig. 7 Transmittance spectra together the maximum $T_M(\lambda)$ and minimum $T_m(\lambda)$ transmittance envelope curves of samples: **a** Ta_2O_5 before annealing (1.3×10^{-4} mbar), **b** Ta_2O_5 annealed at 300 °C (1.3×10^{-4} mbar), **c** Ta_2O_5 before annealing (2×10^{-4} mbar), **d** Ta_2O_5 annealed at 300 °C (2×10^{-4} mbar)

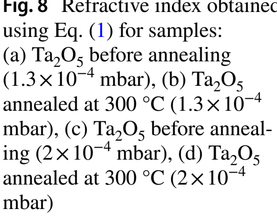
Fig. 8 Refractive index obtained using Eq. (1) for samples: (a) Ta_2O_5 before annealing (1.3×10^{-4} mbar), (b) Ta_2O_5 annealed at 300 °C (1.3×10^{-4} mbar), (c) Ta_2O_5 before annealing (2×10^{-4} mbar), (d) Ta_2O_5 annealed at 300 °C (2×10^{-4} mbar)

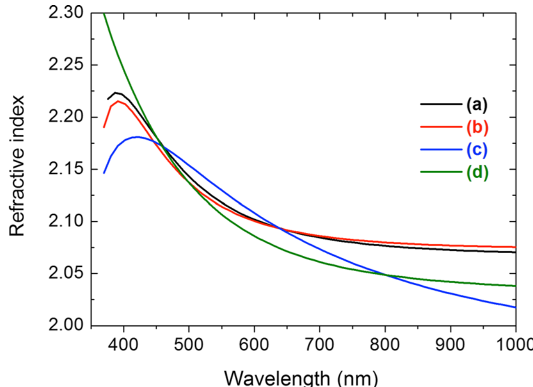

deviations are shown in Table 3. Such values are in good agreement with the monitored thickness during the growth of the samples.

Figure 9 depicts the Tauc´s plot analysis of untreated and annealed samples. These data show the optical band gap energy of the four samples, which is about 3.9 eV for samples

Table 3 The average of the film thickness values with the standard deviations

Sample	Film thickness (nm)
(a) Ta_2O_5 before annealing (1.3×10^{-4} mbar)	369 ± 14
(b) Ta_2O_5 annealed at 300 °C (1.3×10^{-4} mbar)	407 ± 28
(c) Ta_2O_5 before annealing (2×10^{-4} mbar)	403 ± 29
(d) Ta_2O_5 annealed at 300 °C (2×10^{-4} mbar)	370 ± 21

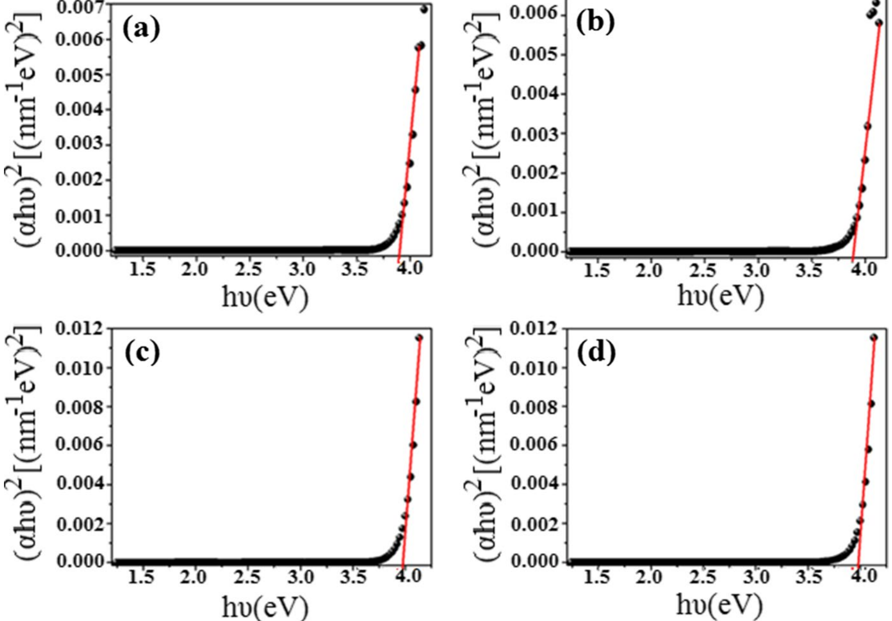

Fig. 9 Tauc plot of **a** Ta_2O_5 before annealing (1.3×10^{-4} mbar), **b** Ta_2O_5 annealed at 300 °C (1.3×10^{-4} mbar), **c** Ta_2O_5 before annealing (2×10^{-4} mbar), **d** Ta_2O_5 annealed at 300 °C (2×10^{-4} mbar)

Table 4 The band gap and Urbach energies obtained from the UV–Visible spectra

Sample name	Band gap (eV)	Urbach energy (meV)
Ta_2O_5 before annealing (1.3×10^{-4} mbar)	3.90	163
Ta_2O_5 annealed at 300 °C (1.3×10^{-4} mbar)	3.88	190
Ta_2O before annealing (2×10^{-4} mbar)	3.98	160
Ta_2Oannealedat 300 °C (2×10^{-4} mbar)	3.97	175

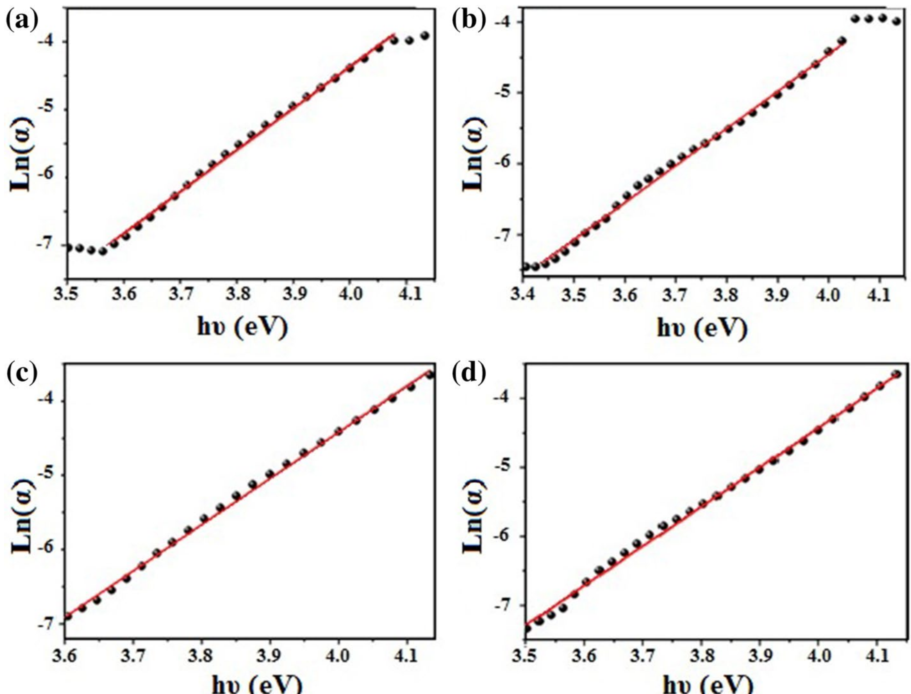

Fig. 10 The Urbach plot of **a** Ta_2O_5 before annealing (1.3×10^{-4} mbar), **b** Ta_2O_5 annealed at 300 °C (1.3×10^{-4} mbar), **c** Ta_2O_5 before annealing (2×10^{-4} mbar) and **d** Ta_2O_5 annealed at 300 °C (2×10^{-4} mbar). Straight lines are linear fit to the data

prepared at working pressure of 1.3×10^{-4} mbar, and around 4 eV for samples prepared at working pressure of 2×10^{-4} mbar (Table 4).

In agreement with the Eq. (5), the Urbach energy can be measured as the slope of the linear dependence of $ln(\alpha)$ on the photon energy (Ghobadi and Rezaee 2016). Figure 10 shows these Urbach plots of the samples before and after the annealing treatments. Both band gap and Urbach energies obtained from the UV–Visible spectra are computed in Table 4.

4 Conclusions

The 3-D surface micromorphology of the Ta_2O_5 thin films deposited on glass substrates by electron gun method and their characteristics were determined using a variety of instruments and methodologies. The 3-D surface microtexture of all samples highlighted multifractal properties characterized by the generalized dimension D_q and the singularity spectrum $f(\alpha)$. It was found that the most irregular topography was found for samples Ta_2O_5 before annealing (1.3×10^{-4} mbar) ($\Delta\alpha=0.129$), while the most regular topography was found for samples Ta_2O_5 before annealing (2×10^{-4} mbar) ($\Delta\alpha=0.052$). Furthermore, the right arm of $f(\alpha)$ is associated with flat zones, while the left arm of $f(\alpha)$ is associated with strongly irregular areas. Also, for all samples, the right shoulder of the singularity spectrum $f(\alpha)$ is much longer than the left shoulder. Furthermore, the annealing process

influences the film thicknesses. The smallest size of thickness was observed for Ta_2O_5 before annealing (1.3×10^{-4} mbar) sample (t = 369 ± 14 nm), while the highest thickness was observed for Ta_2O_5 annealed at 300 °C (1.3×10^{-4} mbar) sample (t = 407 ± 28 nm). The optical analyses combined with the multifractal studies provided a deeper analysis that can serve as a foundation for the development of novel micro-topography models of Ta_2O_5 thin films deposited on glass substrates by electron gun method.

Compliance with ethical standards

Conflict of interest Neither author has a financial or proprietary interest in any material or method mentioned. The authors declare that they have no competing interests.

References

Alijani, M., Kaleji, B.K., Rezaee, S.: Improved visible light photocatalytic activity of TiO_2 nano powders with metal ions doping for glazed ceramic tiles. Opt. Quantum Electron. **49**, 225 (2017). https://doi.org/10.1007/s11082-017-1064-x

Arman, A., Ţălu, Ş., Luna, C., Ahmadpourian, A., Naseri, M., Molamohammadi, M.: Micromorphology characterization of copper thin films by AFM and fractal analysis. J. Mater. Sci.: Mater. Electron. **26**(12), 9630–9639 (2015). https://doi.org/10.1007/s10854-015-3628-5

Chaneliere, C., Autran, J.L., Devine, R.A.B., Balland, B.: Tantalum pentoxide (Ta_2O_5) thin films for advanced dielectric applications. Mater. Sci. Eng. R Rep. **22**(6), 269–322 (1998). https://doi.org/10.1016/S0927-796X(97)00023-5

Chen, P.W., Chang, C.T., Manirul Ali, Md., Wu, J.Y., Li, Y.C., Chen, M.H., Jan, D.J., Yuan, C.T.: Tantalum oxide film deposited by vacuum cathodic arc plasma with improved electrochromic performance. Sol. Energy Mater. Sol. Cells **182**, 188–195 (2018). https://doi.org/10.1016/j.solmat.2018.02.034

Chhabra, A.B., Meneveau, C., Jensen, R.V., Sreenivasan, K.R.: Direct determination of the f(α) singularity spectrum and its application to fully developed turbulence. Phys. Rev. A **40**(9), 5284–5293 (1989). https://doi.org/10.1103/PhysRevA.40.5284

Dallaeva, D., Ţălu, Ş., Stach, S., Škarvada, P., Tomanek, P., Grmela, L.: AFM imaging and fractal analysis of surface roughness of AlN epilayers on sapphire substrates. Appl. Surf. Sci. **312**, 81–86 (2014). https://doi.org/10.1016/j.apsusc.2014.05.086

Dastan, D., Panahi, S.L., Chaure, N.B.: Characterization of titania thin films grown by dip-coating technique. J. Mater. Sci.: Mater. Electron. **27**, 12291–12296 (2016). https://doi.org/10.1007/s10854-016-4985-4

Ghobadi, N., Rezaee, S.: Synthesis of Ag–Cu–Pd alloy by DC-magnetron sputtering: micromorphology analysis. J. Mater. Sci.: Mater. Electron. **27**(8), 8464–8477 (2016). https://doi.org/10.1007/s10854-016-4861-2

Han, J., Li, Y., Fan, W., He, C., Wang, P., Feng, G., Guo, C.: The ablation of Ta_2O_5 film by pulsed nanosecond Gaussian laser beams. Optik **126**(20), 2327–2330 (2015). https://doi.org/10.1016/j.ijleo.2015.05.127

Ilican, S., Caglar, Y., Caglar, M.: Preparation and characterization of ZnO thin films deposited by sol–gel spin coating method. J. Optoelectron. Adv. Mater. **10**, 2578–2583 (2008)

Kaliwoh, N., Zhang, J., Boyd, I.W.: $(Ta_2O_5)1-x(TiO_2)_x$ deposited by photo-induced CVD using 222 nm excimer lamps. Appl. Surf. Sci. **186**(1–4), 246–250 (2002). https://doi.org/10.1016/S0169-4332(01)00601-8

Kaspar, P., Sobola, D., Dallaev, R., Ramazanov, S., Nebojsa, A., Rezaee, S., Grmela, L.: Characterization of Fe_2O_3 thin film on highly oriented pyrolytic graphite by AFM, Ellipsometry and XPS. Appl. Surf. Sci. **493**, 673–678 (2019). https://doi.org/10.1016/j.apsusc.2019.07.058

Konsek, D., Stach, S., Ţălu, Ş., Naderi, S., Arman, A.: Correlation between 3-D surface topography and different deposition times of engineered Ni@a-C: H thin films. Silicon **10**(5), 2141–2151 (2018). https://doi.org/10.1007/s12633-017-9743-6

Korpi, A.G., Rezaee, S., Luna, C., Ţălu, Ş., Arman, A., Ahmadpourian, A.: Influence of the oxygen partial pressure on the growth and optical properties of RF-sputtered anatase TiO_2 thin films. Results Phys. **7**, 3349–3352 (2017). https://doi.org/10.1016/j.rinp.2017.08.018

Korpi, A.G., Ţălu, Ş., Bramowicz, M., Arman, A., Kulesza, S., Pszczolkowski, B., Jurečka, S., Mardani, M., Luna, C., Balashabadi, P., Rezaee, S., Gopikishan, S.: Minkowski functional characterization and fractal analysis of surfaces of titanium nitride films. Mater. Res. Express **6**(8), 1–14 (2019). https://doi.org/10.1088/2053-1591/ab26be

Lee, J.S., Chang, S.J., Chen, J.F., Sun, S.C., Liu, C.H., Liaw, U.H.: Effects of O_2 thermal annealing on the properties of CVD Ta_2O_5 thin films. Mater. Chem. Phys. **77**(1), 242–247 (2003). https://doi.org/10.1016/S0254-0584(01)00559-4

Lin, J., Suzuki, T., Matsunaga, D., Hieda, K.: Low crystallization temperature for Ta_2O_5 thin films. Jpn. J. Appl. Phys. **42**(11), 7023–7024 (2003). https://doi.org/10.1143/JJAP.42.7023

Luna, C., Cuan-Guerra, A.D., Barriga-Castro, E.D., Núñez, N.O., Mendoza-Reséndez, R.: Confinement and surface effects on the physical properties of rhombohedral-shape hematite (α-Fe_2O_3) nanocrystals. Mater. Res. Bull. **80**, 44–52 (2016). https://doi.org/10.1016/j.materresbull.2016.03.029

Mikhelashvili, V., Eisenstein, G.: Electrical characteristics of Ta_2O_5 thin films deposited by electron beam gun evaporation. Appl. Phys. Lett. **75**(18), 2836–2838 (1999). https://doi.org/10.1063/1.125166

Mwema, F.M., Oladijo, O.P., Sathiaraj, T.S., Akinlabi, E.T.: Atomic force microscopy analysis of surface topography of pure thin aluminium films. Mater. Res. Express **5**(4), 1–15 (2018). https://doi.org/10.1088/2053-1591/aabe1b

Mwema, F.M., Akinlabi, E.T., Oladijo, O.P.: Fractal analysis of hillocks: a case of RF sputtered aluminum thin films. Appl. Surf. Sci. **489**, 614–623 (2019). https://doi.org/10.1016/j.apsusc.2019.05.340

Naseri, N., Solaymani, S., Ghaderi, A., Bramowicz, M., Kulesza, S., Ţălu, Ş., Pourreza, M., Ghasemi, S.: Microstructure, morphology and electrochemical properties of Co nanoflake water oxidation electrocatalyst at micro- and nanoscale. RSC Adv. **7**(21), 12923–12930 (2017). https://doi.org/10.1039/c6ra28795f

Porporati, A., Roitti, S., Sbaizero, O.: Metallorganic chemical vapor deposition of Ta_2O_5 films. J. Eur. Ceram. Soc. **23**(2), 247–251 (2003). https://doi.org/10.1016/S0955-2219(02)00184-X

Porqueras, I., Marti, J., Bertran, E.: Optical and electrical characterisation of Ta_2O_5 thin films for ionic conduction applications. Thin Solid Films **343–344**(6090), 449–452 (1999). https://doi.org/10.1016/S0040-6090(99)00121-2

Prachachet, R., Buranasiri, P., Horprathum, M., Eiamchai, P., Limwichean, S., Patthanasettakul, V., Nuntawong, N., Chindaudom, P., Samransuksamer, B., Lertvanithphol, T.: Investigation of optical characteristics of the evaporated Ta_2O_5 thin films based on ellipsometry and spectroscopy. Mater. Today Proc. **4**(5), 6365–6371 (2017). https://doi.org/10.1016/j.matpr.2017.06.140

Prasanna, S., Shaik, H., Mohan Rao, G., Vandana, Singh, P.K., Jayakumar, S., Balasundaraprabhu, R.: Effect of post-deposition annealing on composition and electrical properties of dc reactive magnetron sputtered Al_2O_3 thin films. Mater. Technol. **29**(2), 83–89 (2014). https://doi.org/10.1179/1753555713Y.0000000108

Rezaee, S., Ghobadi, N.: Synthesis of Ag-Cu-Pd alloy thin films by DC-magnetron sputtering: case study on microstructures and optical properties. Results Phys. **9**, 1148–1154 (2018). https://doi.org/10.1016/j.rinp.2018.04.029

Sánchez-González, J., Díaz-Parralejo, A., Ortiz, A.L., Guiberteau, F.: Determination of optical properties in nanostructured thin films using the Swanepoel method. Appl. Surf. Sci. **252**(17), 6013–6017 (2006). https://doi.org/10.1016/j.apsusc.2005.11.009

Shakoury, R., Grayeli Korpi, A., Ghosh, K., Ţălu, Ş., Rezaee, S., Mwema, F., Mardani, M., Arman, A.: Stereometric and scaling law analysis of surface morphology of stainless steel type AISI 304 coated with Mn: a conventional and fractal evaluation. Mater. Res. Express **6**(11), 116436 (2019). https://doi.org/10.1088/2053-1591/ab4aa6

Shibata, S.: Dielectric constants of Ta_2O_5 thin films deposited by r.f. sputtering. Thin Solid Films **277**(1–2), 1–4 (1996). https://doi.org/10.1016/0040-6090(95)08234-4

Shikhgasan, R., Ţălu, Ş., Dinara, S., Sebastian, S., Guseyn, R.: Epitaxy of silicon carbide on silicon: micromorphological analysis of growth surface evolution. Superlattices Microstruct. **86**, 395–402 (2015). https://doi.org/10.1016/j.spmi.2015.08.007

Siodmiak, M., Frenking, G., Korkin, A.: On the mechanism of chemical vapor deposition of Ta_2O_5 from $TaCl_5$ and H_2O. An ab initio study of gas phase reactions. Mater. Sci. Semicond. Process. **3**(1–2), 65–70 (2000). https://doi.org/10.1016/S1369-8001(00)00010-X

Sobola, D., Ţălu, Ş., Solaymani, S., Grmela, L.: Influence of scanning rate on quality of AFM image: study of surface statistical metrics. Microsc. Res. Tech. **80**(12), 1328–1336 (2017). https://doi.org/10.1002/jemt.22945

Stach, S., Dallaeva, D., Ţălu, Ş., Kaspar, P., Tomanek, P., Giovanzana, S., Grmela, L.: Morphological features in aluminum nitride epilayers prepared by magnetron sputtering. Mater. Sci. Poland **33**, 175–184 (2015). https://doi.org/10.1515/msp-2015-0036

Stach, S., Sapota, W., Ţălu, Ş., Ahmadpourian, A., Luna, C., Ghobadi, N., Arman, A., Ganji, M.: 3D Surface stereometry studies of sputtered TiN thin films obtained at different substrate temperatures. J. Mater. Sci.: Mater. Electron. **28**(2), 2113–2122 (2017). https://doi.org/10.1007/s10854-016-5774-9

Swanepoel, R.: Determination of thethickness and opticalconstants of amorphoussilicon. J. Phys. E: Sci. Instrum. **16**(12), 1214–1222 (1983). https://doi.org/10.1088/0022-3735/16/12/023

Ţălu, Ş.: Micro and Nanoscale Characterization of Three Dimensional Surfaces. Basics and Applications. Napoca Star Publishing House, Cluj-Napoca (2015)

Ţălu, Ş., Marković, Z., Stach, S., Todorović Marković, B., Ţălu, M.: Multifractal characterization of single wall carbon nanotube thin films surface upon exposure to optical parametric oscillator laser irradiation. Appl. Surf. Sci. **289**, 97–106 (2014). https://doi.org/10.1016/j.apsusc.2013.10.114

Ţălu, Ş., Morozov, I.A., Yadav, R.P.: Multifractal analysis of sputtered indium tin oxide thin film surfaces. Appl. Surf. Sci. **65**(3), 294–300 (2019). https://doi.org/10.1016/j.apsusc.2019.04.170

Tian, X., Xiong, S., Zhang, Y., Zhang, K.: Simulation of thermal stress in ion beam sputtered Ta_2O_5/SiO_2 multilayer coatings on different substrates by finite element analysis. Surf. Coat. Technol. **362**, 225–233 (2019). https://doi.org/10.1016/j.surfcoat.2019.02.004

Wang, S.C., Liu, K.Y., Huang, J.L.: Tantalum oxide film prepared by reactive magnetron sputtering deposition for all-solid-state electrochromic device. Thin Solid Films **520**(5), 1454–1459 (2011). https://doi.org/10.1016/j.tsf.2011.08.046

Yadav, R.P., Kumar, M., Mittal, A.K., Pandey, A.C.: Fractal and multifractal characteristics of swift heavy ion induced self-affine nanostructured BaF_2 thin film surfaces. Chaos **25**(8), 083115 (2015). https://doi.org/10.1063/1.4928695

Yoon, S.G., Kim, H.K., Kim, M.J., Lee, H.M., Yoon, D.H.: Effect of substrate temperature on surface roughness and optical properties of Ta_2O_5 using ion-beam sputtering. Thin Solid Films **475**(1–2), 239–242 (2005). https://doi.org/10.1016/j.tsf.2004.07.043

Yoon, S.G., Kang, S.M., Jung, W.S., Kim, S.W., Yoon, D.H.: Effect of assist ion beam voltage on intrinsic stress and optical properties of Ta_2O_5 thin films deposited by dual ion beam sputtering. Thin Solid Films **516**(11), 3582–3585 (2008). https://doi.org/10.1016/j.tsf.2007.08.051

Zavarian, A.A., Ţălu, Ş., Hafezi, F., Achour, A., Luna, C., Naderi, S., Mardani, M., Arman, A., Ahmadpourian, A.: Study of the microstructure and surface morphology of silver nanolayers obtained by ion-beam deposition. J. Mater. Sci.: Mater. Electron. **28**(20), 15293–15301 (2017). https://doi.org/10.1007/s10854-017-7410-8

Publisher's Note Springer Nature remains neutral with regard to jurisdictional claims in published maps and institutional affiliations.

Affiliations

Reza Shakoury[1] · Sahar Rezaee[2] · Fredrick Mwema[3,4] · Carlos Luna[5] · Koushik Ghosh[6] · Stanislav Jurečka[7] · Ştefan Ţălu[8] · Ali Arman[9] · Alireza Grayeli Korpi[10]

[1] Department of Physics, Faculty of Science, Imam Khomeini International University, Qazvin, Iran

[2] Department of Physics, Kermanshah Branch, Islamic Azad University, Kermanshah, Iran

[3] Mechanical Engineering Science, University of Johannesburg, Johannesburg, South Africa

[4] Department of Mechanical Engineering, Dedan Kimathi University of Technology, Nyeri, Kenya

[5] Facultad de Ciencias Físico Matemáticas (FCFM), Universidad Autónoma de Nuevo León (UANL), Av. Universidad s/n, 66455 San Nicolás de los Garza, Nuevo León, Mexico

[6] Department of Pure and Applied Physics, Guru Ghasidas Vishwavidyalaya, Bilaspur, Chhattisgarh 495009, India

[7] Institute of Aurel Stodola, Faculty of Electrical Engineering, University of Žilina, Nálepku 1390, 031 01 Liptovský Mikuláš, Slovakia

[8] The Directorate of Research, Development and Innovation Management (DMCDI), Technical University of Cluj-Napoca, Constantin Daicoviciu St., No. 15, 400020 Cluj-Napoca, Cluj County, Romania

[9] ACECR, Institute of Technology Development, Sharif University Branch, Tehran, Iran

[10] Physics and Accelerators Research School, Nuclear Sciences and Technology Research Institute, Tehran, Iran